Available online at www.sciencedirect.com
SCIENCE DIRECT
Catalysis Today 109 (2005) 205–213
CATALYSIS TODAY
www.elsevier.com/locate/cattod

Pressure and temperature effects on the hydrodynamic characteristics of ebullated-bed systems

R.S. Ruiz [b,*], F. Alonso [a,c], J. Ancheyta [a]

[a] *Instituto Mexicano del Petróleo, Eje Central Lázaro Cárdenas 152, México D.F. 07730, Mexico*
[b] *Area de Ingeniería Química, Universidad Autónoma Metropolitana-Iztapalapa, Av. San Rafael Atlixco #186, Col. Vicentina, México D.F. 09340, Mexico*
[c] *Instituto Tecnológico de Ciudad Madero, Juventino Rosas y Jesús Urueta, Col. Los Mangos, Cd. Madero, Tam. 89440, Mexico*

Available online 6 October 2005

Abstract

Experiments were performed to study the hydrodynamic characteristics of ebullate-bed systems operated under conditions of high pressure and temperature. The effects of these variables on bed porosity and the liquid minimum fluidization velocity were determined and a correlation has been proposed as a criteria for determining flow regime transitions between the dispersed and coalesced bubble flow regimes. The bed porosity has been described with the pseudo-fluid model. The minimum fluidization velocity data were contrasted with predictions from empirical correlations reported in the literature.

Keywords: Hydrodynamics; Ebullated-bed; Pseudo-fluid; Flow regime; Minimum fluidization

1. Introduction

High pressure and high temperature operation is common in industrial three-phase ebullated-bed reactors utilized in hydrotreating processes of residual materials. Knowledge of the hydrodynamic characteristics at severe conditions is critical for predicting the performance of these reactors. Among such characteristics are the incipient liquid fluidization velocity, the bed expansion and the bubble flow regime. Although these properties have been extensively reported in the literature for ambient conditions, little has been reported for systems at high temperature and pressure.

In an ebullated-bed system, at a given gas velocity, bed expansion increases with liquid velocity and/or viscosity. In general, a bed of small particles operated under ambient conditions contracts when a low gas flow rate is first introduced into the liquid–solid fluidized bed [1]. Bed contraction continues with further increases in gas velocity until the bed height reaches a minimum point, beyond which the bed expands with an increase in gas velocity. On the other hand, for a bed of large particles bed contraction does not occur. The bed and expansion phenomena has been described by the generalized wake model developed by Bhatia and Epstein [2], which considers that the effective amount of liquid in the bed available for fluidizing the bed is reduced due to liquid entrainment in the wake of bubbles.

For beds operated at high temperature and pressure either bed expansion or contraction can occur. Blum and Toman [3] operated a nitrogen-light mineral oil-cylindrical catalyst particles three-phase fluidized bed at 6.8 MPa and at temperatures up to 350 °C. They found that the bed height increased continuously with gas flow rate without bed contraction. Jiang et al. [4] utilized a bed of glass beads fluidized with Paratherm NF heat transfer fluid as the liquid phase and nitrogen as the gas phase, which was operated at pressures up to 17.4 MPa and temperatures up to 94 °C. Their results indicated that at low temperatures bed contraction occurred over the entire range of pressure studied. However, the tendency of bed contraction was found to diminish at high temperatures, and to disappear under high temperature and high pressure conditions.

Several studies report that pressure affects the bubble characteristics in ebullated-bed systems. Jiang et al. [5] visually

* Corresponding author. Fax: +52 55 9175 8429.
E-mail address: rmr@xanum.uam.mx (R.S. Ruiz).

0920-5861/$ – see front matter © 2005 Elsevier B.V. All rights reserved.
doi:10.1016/j.cattod.2005.08.019

Nomenclature

Ar_L	liquid Archimedes number, $Ar_L = d_v^3 \rho_L (\rho_S - \rho_L) g/\mu_L^2$
d_b	bubble size (m)
d_c	column diameter (m)
d_e	volume equivalent bubble diameter (m)
d'_e	dimensionless bubble size (m)
d_v	equivalent diameter of sphere having the same volume as the particle (m)
Fr_G	gas Froude number, $Fr_G = U_G^2/gd_v$
g	gravity acceleration (m/s^2)
H_B, H_o	expanded and static bed heights (m)
j_{cd}	gas drift flux (m/s)
Mo	Morton number, $Mo = g\mu_L^4(\rho_L - \rho_G)/\rho_L^2\sigma_L^3$
Mo_L	liquid Morton number, $Mo_L = g\mu_L^4/\rho_L\sigma_L^3$
n	Richardson–Zaki index
P	pressure (MPa)
Re_G	gas Reynolds number, $Re_{LG} = \rho_L d_v U_G/\mu_L$
Re_{Lmf}	liquid Reynolds number at minimum three-phase fluidization $Re_{Lmf} = U_{Lmf} d_v \rho_L/\mu_L$
Re_t	pseudo-fluid Reynolds number based on the terminal velocity, $Re_t = U_t d_v \rho_{pf}/\mu_{pf}$
$U_{b\infty}$	rise velocity of a single bubble in a liquid medium (m/s)
U'_b	dimensionless bubble rise velocity
U_G	gas superficial velocity (m/s)
U_g^o	terminal velocity of a single bubble in the liquid (m/s)
U_L	liquid superficial velocity (m/s)
U_{Lmf}	minimum liquid fluidization velocity of the three-phase bed (m/s)
U_{Lmf}^o	minimum fluidization velocity of the liquid–solid system (m/s)
U_{pf}	velocity of the pseudo-fluid (m/s)
U_s^o	single-particle terminal settling velocity in the pseudo-fluid (m/s)
W_s	catalyst loading (kg)

Greek letters

α	dispersed phase volume fraction
β_G	gas void fraction per unit porous volume
ε	bed porosity
ε_g	gas phase holdup
ε_g^*	gas phase holdup on a solids-free basis
ε_l	liquid phase holdup
ε_l^*	liquid phase holdup on a solids-free basis
ε_{mf}	bed porosity at minimum fluidization
ε_s	solids holdup
ϕ	sphericity factor
μ	dynamic viscosity (Pa/s)
ρ	density (kg/m^3)
σ_L	liquid surface tension (N/m)

Subscripts

C	continuous phase
D	dispersed phase
G, g	gas
L, l	liquid
pf	pseudo-fluid
p	particle
S, s	solid

observed the hydrodynamic behavior of a three-phase fluidized bed at elevated pressures up to 1 MPa and at ambient temperature. The study indicated that bubble size decreases, bubble size distribution narrows, and gas holdup increases with increasing pressure. Luo et al. [6] experimentally studied the phase holdups and heat transfer in three-phase fluidized beds over a pressure range of 0.1–15.6 MPa and at ambient temperature. They also report that bubble size decreases and the bubble size distribution becomes narrower with an increase in pressure. They found that the bubble size reduction leads to an increase in the transition gas velocity from the dispersed bubble regime to the coalesced bubble regime, an increase in the gas holdup, and a decrease in the liquid and solid holdups.

The minimum fluidization velocity represents the smallest superficial liquid velocity, which at a given superficial gas velocity brings particles in the bed from rest to motion. Knowledge of this velocity is of considerable relevance in the design and safe operation of ebullated-bed reactors. A great deal of experimental work has been devoted to investigating the onset of fluidization of three-phase fluidized beds, and hence many correlations and models are found in the literature for its prediction. Most of these studies, however, seem to have been performed under ambient conditions. This is apparent from the work of Larachi et al. [7], who proposed neural network correlations based on a wide historic minimum fluidization velocity database for three-phase systems (with 540 measurements). It can be seen from the operating conditions reported that all of the data utilized correspond to experimental work obtained at a pressure of 0.1 MPa and a temperature range of 20–39 °C. One of the few studies in the open literature that considers high temperature and high pressure on the incipient fluidization velocity is that of Jiang et al. [8]. They conducted experiments at pressures up to 17 MPa and temperatures up to 135 °C, and for which it was reported that the minimum fluidization velocity decreases with an increase in pressure and a decrease in temperature. It was also observed that pressure effects become insignificant when the pressure reaches a certain value and large bubbles disappear.

The aim of this contribution is to examine the effect of pressure and temperature on the hydrodynamics properties of ebullated-bed systems. Specifically, the bed porosity, and the liquid minimum fluidization velocity have been measured and compared with the predictions of well-known equations and models developed for ambient conditions. The effect of temperature and pressure on the bubble flow regime has been analyzed and an empirical correlation is proposed to predict the bubble flow transition gas velocity between the dispersed and the coalesced bubble regimes at high pressures.

2. Experimental

The reaction section of a hydrotreating pilot plant was utilized in the determination of experimental hydrodynamic data at high pressure and temperature conditions and which has been described elsewhere [9]. An schematic diagram of the experimental system is shown in Fig. 1. The reactor consisted of an ebullated-bed within a vertical tube 434 cm high and 2.94 cm in diameter, and with a settled bed height of 135 cm. The system has been designed to operate at severe conditions of temperature and pressure and so pressures and temperatures of up to 15 MPa and 100 °C, respectively, have been considered. The bed consisted of 1.71 mm diameter glass beads, 2509 kg/m^3 density, supported by a wire mesh placed at the bottom of the reactor, fluidized by co-current diesel fuel ($\mu_1 = 45 \times 10^{-4}$ kg/(m s), $\sigma = 30 \times 10^{-3}$ N/m and $\rho_1 = 836$ kg/m^3 at 20 °C and 0.1 MPa) and nitrogen flows. Superficial gas velocities of up to 0.014 and 0.016 m/s were used, respectively, for the gas and liquid flow rates. Bed density profiles were obtained with a commercial gamma-ray densitometry SGD Density System unit from TN Technologies. The system basically consists of a nuclear density gauge mounted in a movable assembly mechanism, which was used to transport the gauge axially along the column. The gauge is comprised of a Cesium-137 source contained in a lead-filled, steel-encased housing mounted on one side of the bed, and a scintillation detector, which is mounted on the opposite side of the column. For calculation of the bed density at a given height, the system has to be previously calibrated with a fluid of known density, and then it utilizes the attenuation coefficient of the process material components to compute the response to process density changes. From the bed density profiles the average bed densities, ρ_B, were determined. The expanded bed heights, H_B, were obtained from the position where there was an abrupt change in the column axial density profile, which corresponded to the density change at the bed–freeboard interface.

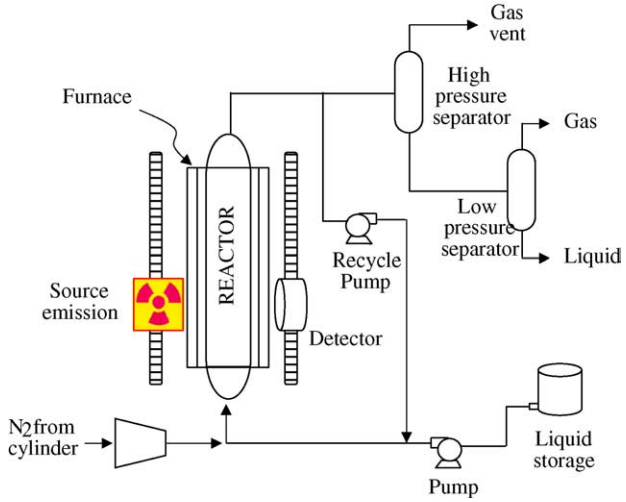

Fig. 1. Schematic diagram of the experimental system.

The overall solids holdup is related to the expanded bed height by

$$\varepsilon_s = \frac{4W_s}{\pi d_c^2 \rho_s H_B} \quad (1)$$

The liquid and gas holdups are then determined from solving the following equations

$$\rho_B = \rho_s \varepsilon_s + \rho_l \varepsilon_l + \rho_g \varepsilon_g \quad (2)$$

$$\varepsilon_g + \varepsilon_l + \varepsilon_s = 1 \quad (3)$$

3. Experimental results and discussion

3.1. Bed expansion

In conducting high pressures and high temperatures experiments, the bed is first fluidized by the liquid, and then the gas is introduced into the bed. The bed height is determined from the density profile of the reactor and the bed porosity is then calculated using Eq. (1). For ebullated-beds operated under ambient conditions at a given gas velocity, the bed porosity increases with an increase in the liquid flow rate as well as with an increase in the liquid viscosity. Furthermore, at a given liquid velocity, upon introduction of the gas phase the bed porosity can either decrease or increase depending on the bubble flow pattern. The same phenomenon is observed in systems at high pressure. Fig. 2 shows the experimental bed porosity for 1.7 mm glass beads as a function of gas velocity at two pressures and 20 °C. As it can be seen from this figure, for both pressures the bed porosity increases with gas velocity. It is also apparent that the porosity increases when pressure is increased from 7.5 to 15 MPa. An increase in porosity (or bed height) with gas velocity, as observed in Fig. 2, is typical of fluidized systems under the so called dispersed bubble flow regime, the main characteristic of which is

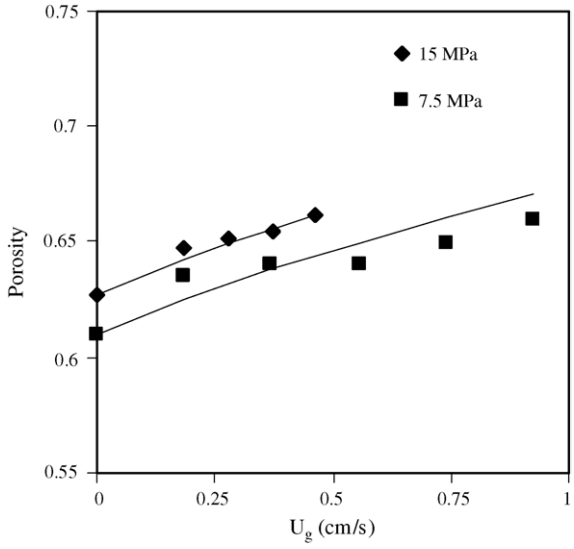

Fig. 2. Effect of gas velocity on the bed porosity at two different pressures, $U_l = 1.4$ cm/s and 20 °C.

the presence of relatively small bubbles uniformly distributed in the column. This seems to be in accordance with visual observations of bubbles at the bed surface of high pressure systems [4], which showed that the mean size of bubbles decreases significantly and their distribution becomes much narrower when the pressure is increased from 1.8 to 17.4 MPa.

Similar results were obtained for the bed operated at 100 °C. As it is shown in Fig. 3, the bed porosity at this temperature also increases with an increase in gas velocity, and therefore a continuous bed expansion was observed. It is also evident that the porosity decreases when the temperature is increased from 20 to 100 °C. For the diesel fuel at 150 MPa, an increase in temperature from 20 to 100 °C yields a reduction of both viscosity and density of about 70 and 6%, respectively. The reduction of liquid viscosity will reduce the drag force on the particles exerted by the fluid, while the reduction in its density will reduce the buoyancy force on the particles. A decrease in both of these forces leads to a decrease in the bed porosity.

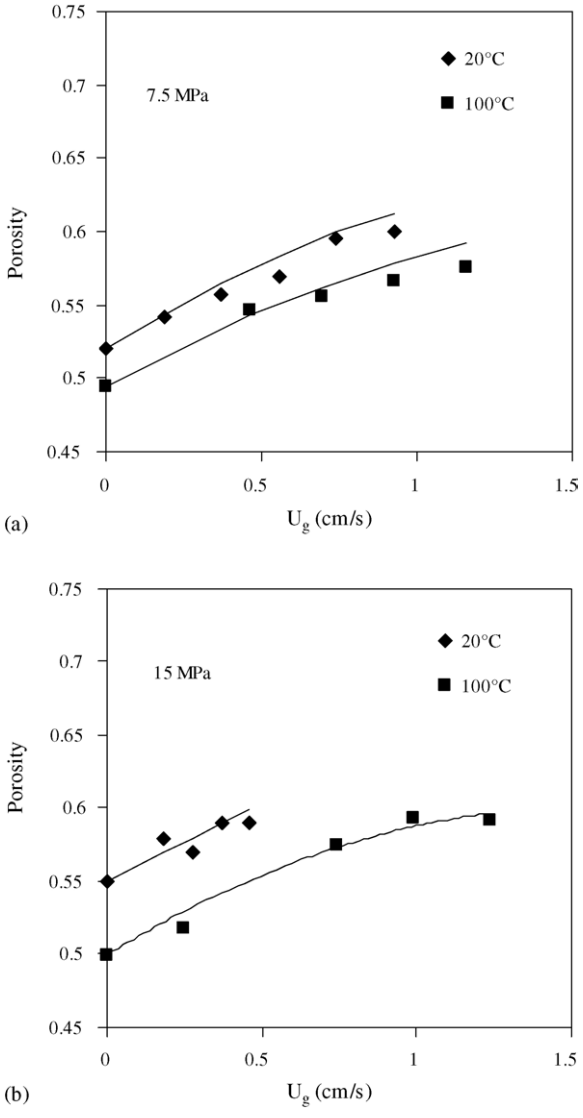

Fig. 3. Effect of gas velocity on the bed porosity at two different temperatures, $U_l = 0.7$ cm/s and (a) 7.5 MPa and (b) 15.0 MPa.

The effects of pressure and temperature on the bed expansion has been modeled in the present work based on the pseudo-fluid model utilized by Di Felice [10] for the prediction of phase holdups in three-phase fluidization at atmospheric conditions in the dispersed flow regime. In this model, the liquid and gas phases are treated as a single homogeneous fluid whose characteristics, such as density, viscosity and flow rate are determined independently. These characteristics of the hypothetical fluid must be such that they will give the same overall interaction effects on the dispersed particle phase, and which can be obtained from the weighted averages of liquid and gas, that is:

$$\rho_{pf} = \varepsilon_l^* \rho_l + \varepsilon_g^*, \tag{4}$$

$$\mu_{pf} = \mu_l(1 + \varepsilon_g^*), \tag{5}$$

$$U_{pf} = U_l + U_g \tag{6}$$

where ε_l^* and ε_g^* are the liquid and gas holdups on a solids-free basis. Eq. (5) has been obtained from the theoretical relationship reported for a suspension of fluid spheres at low concentration [11]:

$$\mu = \mu_C\left(1 + 2.5\alpha\frac{\mu_D + 0.4\mu_C}{\mu_D + \mu_C}\right) \tag{7}$$

where the subscript D refers to the dispersed phase, the subscript C refers to the continuous phase and α is the dispersed phase volume fraction. For a gas–liquid systems, with the gas being the dispersed phase, Eq. (7) reduces to Eq. (5) when μ_D is negligible compared with μ_C.

The solid phase holdup can be predicted from the pseudo-fluid characteristics assuming that the voidage and velocity relationship follows the Richardson and Zaki equation [12]

$$\varepsilon = \left(\frac{U_{pf}}{U_s^o}\right)^{1/n} \tag{8}$$

where U_s^o, the single-particle terminal settling velocity in the pseudo-fluid, is estimated from the correlation given by Schlichting [13] as

$$U_s^o = \left[0.072\frac{d_v^{1.6}(\rho_p - \rho_{pf})g}{\rho_{pf}^{0.4}\mu_{pf}^{0.6}}\right]^{1/1.4} \quad 2 < Re_t < 500. \tag{9}$$

In the present work, the index n in Eq. (8) was obtained from porosity data of the liquid–solid system.

According to the approach proposed by Di Felice [10], the system becomes completely predictive once the system conditions are known and the values of ε_l^* and ε_g^* have been estimated. For estimating $\varepsilon_l^*$and ε_g^* it is assumed that the gas–liquid system is unaffected by the presence of the solid particles, apart in the reduction they cause in the flow area. In order to relate the gas and liquid holdups to their flow rates, Di

Felice utilized the following expression proposed by Wallis [11]

$$U_g(1-\varepsilon_g^*) - U_l\varepsilon_g^* = U_g^o\varepsilon_g^*(1-\varepsilon_g^*)^2 \quad (10)$$

where U_g^o is the terminal velocity of a single bubble in the liquid. In the present work, this velocity has been calculated by the following expression [4,14] for the rise velocity of a single bubble in a liquid medium, $U_{b\infty}$, which has been found to work well at high pressure conditions [15]

$$U_b' = \left[\left(\frac{\mathrm{Mo}^{-1/4}}{13.58}d_e'\right)^{-1.6} + \left(\frac{2.8}{d_e'} + \frac{d_e'}{2}\right)^{-0.8}\right]^{-1/1.6} \quad (11)$$

where

$$U_b' = U_{b\infty}(d_b)\left(\frac{\rho_l - \rho_g}{\sigma g}\right)^{1.4} \quad (12a)$$

$$d_e' = d_e\left[\frac{(\rho_l - \rho_g)g}{\sigma}\right]^{1/2}. \quad (12b)$$

The size of the single bubble used in the above correlation was assumed to be equal to the size of bubbles in the dispersed flow regime, this was estimated to be similar to the size of the smaller bubbles observed in bubble size distributions at high pressures [4], and which was approximately of the order of 1.7 mm.

The predictions of the pseudo-fluid model of the bed porosity of ebullated-bed systems operated at different conditions are shown as a line in Figs. 2 and 3. It is seen that the model can predict reasonably well the experimental data at different temperature and pressures. These results suggest that in the experimental systems described the gas and liquid could be considered homogeneous from the particle point of view. These systems have been found to expand monotonically with gas superficial velocity, which is a characteristic of systems in the dispersed bubble flow regime. The pseudo-fluid model also predicts a continuous bed expansion with gas velocity and it has been reported that its application is limited to the dispersed bubble regime [10]; therefore, it would seem to be inadequate to utilize this model for systems that show a bed contraction upon introduction of the gas phase into the liquid–solid system.

3.2. Flow regime

Ebullated-beds operated at relatively low gas and liquid velocities tend to contain small bubbles with a narrow size distribution, strongly dependent on the gas distributor [16]. Under such conditions the number of bubbles and the gas holdup are also small. As gas velocity is increased, larger bubbles of wider size distribution are encountered. An increase in bubble population decreases the distance between them, which favors their coalescence. Such global behavior of the bed is referred to as coalesced bubble flow.

On the other hand, as liquid flow is increased at a constant low gas flow rate, bubbles become smaller with a narrower size distribution. This is known as the dispersed bubble flow regime.

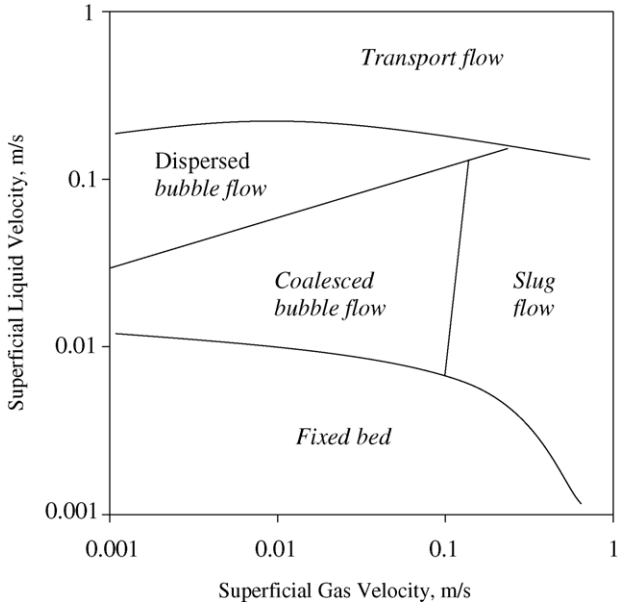

Fig. 4. Schematic diagram of a map regime of a three-phase fluidized bed.

Fig. 4 presents a schematic representation of a map regime similar to the experimental one reported by Zhang et al. [16] for the air–water system with 1.5 mm glass beads. Different flow regimes are presented in this figure as well as the border between them. It is clear from it that an increase in the superficial gas velocity can change the flow regime from the dispersed bubble flow to the coalesced bubble flow regime. Furthermore, the three-phase system can move from the coalesced bubble regime to the dispersed bubble regime as the liquid superficial velocity is increased.

Based on bubble characteristics, Zhang et al. [16] have presented experimental criteria for the identification of the different flow regimes and the transition between them. For the air–water system with spherical particles, at atmospheric pressure, they report the following empirical equation for the liquid transition velocity to the dispersed bubble flow regime:

$$\frac{U_g}{U_l} = 0.721\mathrm{Fr}_g^{0.339}\mathrm{Ar}_l^{0.0746}\left(\frac{\rho_s}{\rho_l}\right)^{-0.667}. \quad (13)$$

The gas drift flux concept has been utilized by many researchers for analyzing the transition between the bubble dispersed and the coalesced bubble regimes in three-phase fluidized beds [6,17,18]. For gas–liquid flows, the drift flux of gas is defined as the volumetric flux of gas relative to surface moving at the average velocity of the two phases [11]. This definition was extended to three-phase fluidized beds [1,17] and can be expressed by

$$j_{cd} = \frac{1-\varepsilon_g}{\varepsilon_l}(U_g\varepsilon_l - U_l\varepsilon_g). \quad (14)$$

where j_{cd} is the gas drift flux, which increases with gas holdup in the dispersed bubble flow regime, however, it appears to

increase at a much higher rate in the coalesced bubble regime. In the present work, the gas drift flux has been determined at elevated pressures as shown in Fig. 5. It seems from this plot that j_{cd} increases with gas holdup at a higher rate at a relatively low pressure of 1 MPa than it appears at 7.5 and 15 MPa, and therefore, at 1 MPa larger and faster bubbles will be expected than in the beds operated at the higher pressures. It is also apparent from Fig. 5 that the differences between the gas drift flux data for the pressures 7.5 and 15 MPa, are significantly smaller than those with the corresponding data at 1 MPa. From the relatively low rate of increase of the drift flux with gas holdup at 7.5 and 15 MPa it appears that the experimental systems were under the dispersed bubble flow regime. These results agree well with those reported by Luo et al. [6] who found an increase with pressure of the transition gas velocity between the coalesced and dispersed bubble flow regimes. Additionally, they observed that this effect was important mainly at pressures below 6 MPa and that at higher pressures the effect would tend to level off.

Luo et al. [6] utilized the gas drift flux concept and reported transition gas velocities at elevated pressures. The experimental data for systems at pressures in the range 0.79–15.6 MPa have been compared with the corresponding predictions obtained with Eq. (13) and the results are presented in Fig. 6. It is clear from this figure that the experimental ratio between the transition gas and liquid velocities is much larger than the corresponding value predicted by above-mentioned equation. That is, at high pressures, for a given liquid velocity much larger gas velocities than those predicted by Eq. (13) can be utilized before the transition between the dispersed and coalesced bubble flow regimes occur. This equation has been obtained from experimental data at atmospheric pressure, and therefore it is probably not surprising that it had failed to predict the transition under high pressure conditions. Nevertheless, it has been observed that the prediction error tends to decrease as the operating pressure is decreased (the smallest errors in Fig. 6 correspond to predictions of the data at 0.79 MPa).

It is evident that correlations that do not take into consideration the effect of pressure on bubble behavior will fail to predict the flow transition velocities at high pressures. Unfortunately, there seems to be very little amount of work published on this regard and as a result no correlation has been found published in the open literature for predicting flow regime transitions at high pressures. Therefore, as an attempt to start fulfilling the necessity of this kind of expressions, in the present work a correlation for the prediction of the transition between the dispersed bubble flow regime and the coalesced bubble regime at elevated pressures is presented in Eq. (15a) and (15). These correlations have been obtained from fitting experimental data published in the literature [6] to an expression similar to that proposed by Zhang et al. [16]. The pressure range of the experimental data considered was from 5.6 to 15.6 MPa, as similar pressures are often employed in ebullated-bed reactors in the hydroprocessing of heavy oil fractions.

The correlations obtained for each of the particle sizes reported in [6] are as follows:

For 2.1 mm diameter particles,

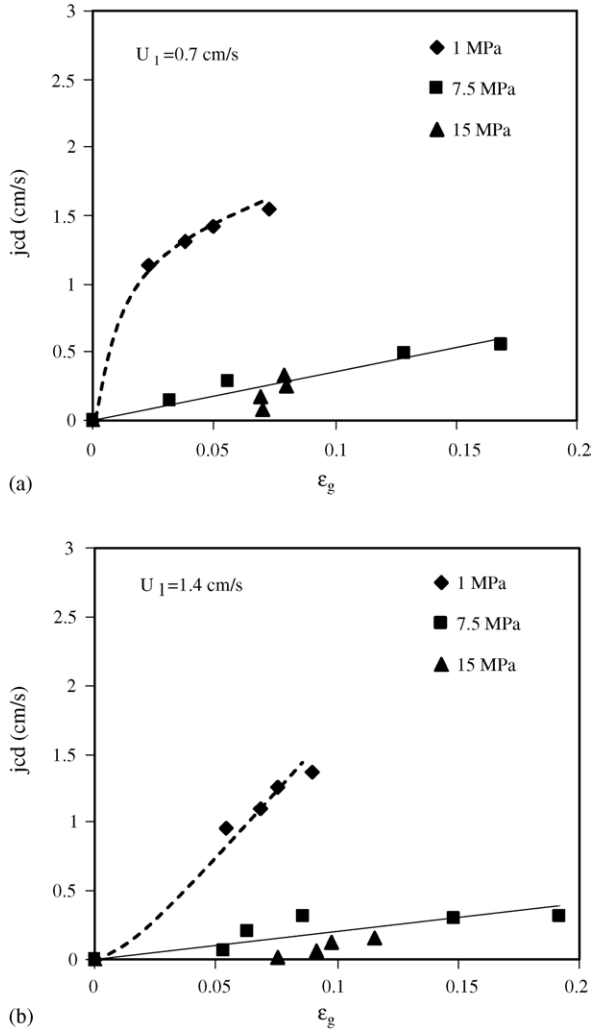

Fig. 5. Effect of gas holdup on the bubble drift flux at different pressures and (a) $U_l = 0.7$ cm/s and (b) $U_l = 1.4$ cm/s.

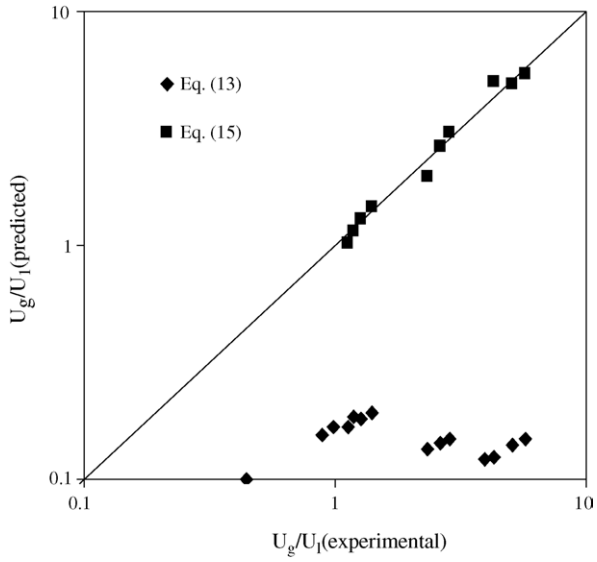

Fig. 6. Experimental gas velocity to liquid velocity ratios from Luo et al. [15] and predicted values.

$$\frac{U_g}{U_l} = 0.756 \mathrm{Fr}_g^n \mathrm{Ar}_l^{-0.8321} \left(\frac{\rho_s}{\rho_l}\right)^{-0.667}. \quad (15a)$$

where

$$n = -0.2241\left(\frac{P}{P_0}\right) - 1.1566$$

and

$15.6\,\mathrm{MPa} \geq P \geq 10.1\,\mathrm{MPa}$.

For 3.0 mm diameter particles,

$$\frac{U_g}{U_l} = 3.41 \times 10^3 \mathrm{Fr}_g^{-1.0} \mathrm{Ar}_l^{-1.7259} \left(\frac{\rho_s}{\rho_l}\right)^{-0.667}. \quad (15b)$$

Which is good for the following pressure range $15.6\,\mathrm{MPa} \geq P \geq P_0 = 5.62\,\mathrm{MPa}$.

In Fig. 6, a comparison is shown between the predicted values obtained with Eq. (15) and data of Luo et al. [6] and from which it is clear that a good correspondence exists between both of them. Eq. (15) has also been utilized for calculating the transition gas velocity for the experimental systems considered in the present work and the results are presented in Fig. 7. The data points that lie on the right hand side of the straight line correspond to the experimental conditions that are in the dispersed bubble flow regime while for those on the left hand side the gas velocity is somewhat higher than the predicted one for the transition between the dispersed and the coalesced bubble flow regimes. The latter correspond to the systems operated at 7.5 MPa and the higher gas velocities considered. According to this figure, it can be said that that most of the experimental systems reported seem to be at the dispersed bubble flow regime, which is consistent with the results reported in Section 3.1 where a good correspondence was found with the pseudo-fluid model.

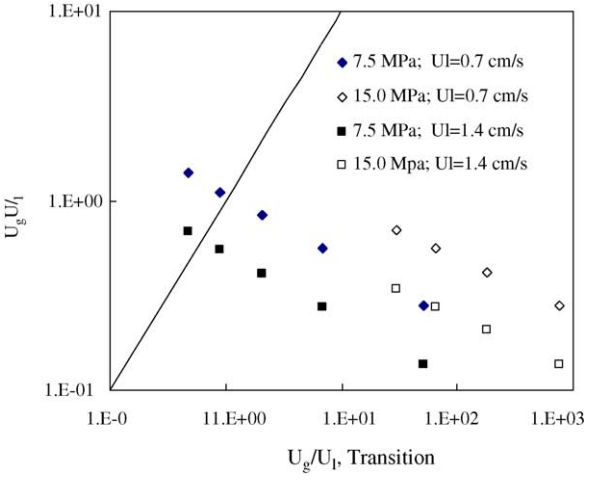

Fig. 7. Experimental gas velocity to liquid velocity ratio and the corresponding ratio at the transition between the dispersed and the coalesced bubble flow regimes, as predicted by Eq. (15a) and (15).

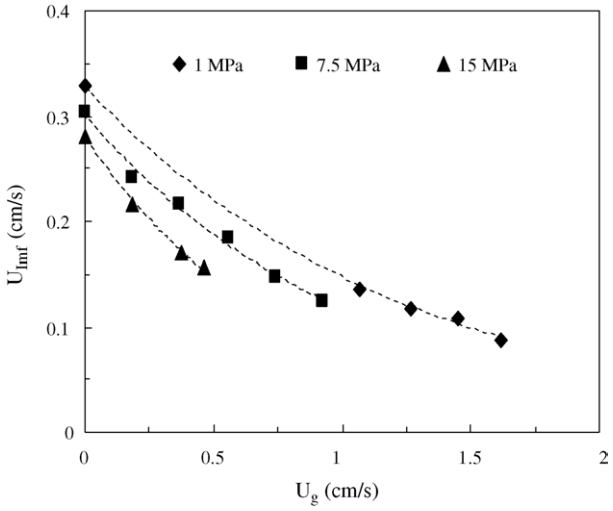

Fig. 8. Effect of gas velocity on the liquid minimum fluidization velocity at different pressures.

3.3. Minimum fluidization velocity

Fig. 8 shows the effect of gas velocity and pressure on the minimum fluidization velocity at 20 °C. As it can be seen, at zero gas flow rate conditions the minimum fluidization velocity appears to decrease with an increase in pressure. This result is due to the fact that the liquid viscosity increases with pressure. It is also evident from Fig. 8 that for the three pressures considered an increase in gas velocity decreases the incipient liquid fluidization velocity. The same behavior has been reported for systems operated at atmospheric pressure. It seems that the presence of gas reduces the liquid holdup, and hence increases the interstitial liquid velocity. This in turn increases the drag exerted on the particles, which leads to earlier fluidization.

As it is shown in Fig. 8, for a given gas velocity the minimum fluidization velocity seems to decrease with an increase in the operating pressure. The effect of pressure can be explained in terms of its impact on liquid properties and bubble behavior. As mentioned above, an increase in pressure increases the liquid viscosity, which in turn increases the drag forces on the particles. With regards to bubble behavior, experimental studies [6] have shown that an increase in pressure tends to produce breakage of large bubbles that leads to systems characterized by the presence small bubbles of uniform size. Bubble breakage produces smaller and slower bubbles that increases the gas holdup, reduces the liquid holdup, and increases the interstitial liquid velocity, which in turn increases the interaction forces between liquid and particles. Based on the foregoing discussion it can be said that an increase in pressure reduces the minimum fluidization velocity by an increase in the drag force exerted on the particles due to an increase of the liquid viscosity and interstitial velocity.

The effect of gas velocity on the minimum fluidization velocity normalized by the corresponding velocity for the liquid–solid system is shown in Fig. 9 for different operating pressures. It appears from this figure that as the pressure is increased the rate at which the ratio $U_{\mathrm{Lmf}}/U^o_{\mathrm{Lmf}}$ varies with gas

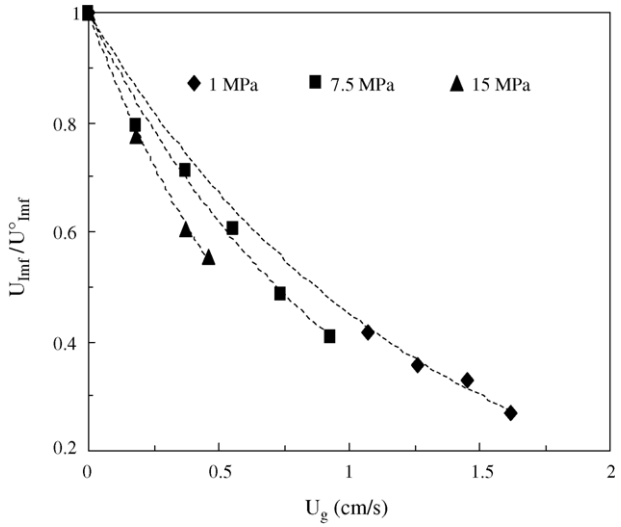

Fig. 9. Effect of gas velocity on the ratio between the incipient fluidization velocity at a high pressure and the one at atmospheric pressure.

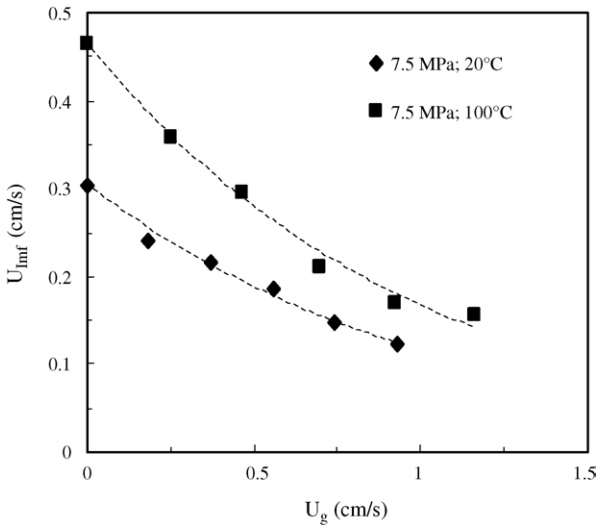

Fig. 10. Effect of gas velocity on the liquid minimum fluidization velocity at two different temperatures.

velocity also increases. Furthermore, for the data considered, the differences between the normalized fluidization velocities at the different pressures seem to increase with gas velocity. These observations appear to be due to the fact that an increase in gas velocity tends to increase the number of large bubbles and that pressure mostly affects these bubbles rather than the small ones [5]. Therefore, appreciable pressure effects on the minimum fluidization velocity can be expected for systems with large bubbles.

Fig. 10 shows the effect of gas velocity pressure on the minimum fluidization velocity at 7.5 MPa and two different temperatures. It is clear from this figure that an increase in temperature increases the minimum fluidization velocity, mainly at low gas velocities and for the liquid–solid system. It is also apparent from both curves in Fig. 10 that the differences between them tend to decease with an increase in gas velocity. For the liquid–solid system an increase in temperature decreases the liquid viscosity, which in turn reduces the drag forces on the particles. For three-phase systems temperature will affect both liquid and gas–liquid interfacial properties. That is on the one hand an increase in temperature reduces the frictional forces on the particles, and on the other the associated decreases of viscosity and surface tension reduce the stability of the gas–liquid interface, which results in a reduction of bubble size [4,8]. As was mentioned before, bubble breakage produces smaller and slower bubbles that reduces the liquid holdup and increases the interstitial liquid velocity, which in turn increases the interaction forces between liquid and particles. This temperature effect associated with bubble size reduction can be expected to be more significant at larger velocities where larger bubbles are more likely to be present in the system. With regard to the temperature effect, it seems that there are two competitive factors that affect the minimum fluidization velocity. One is that a temperature increase reduces the liquid viscosity and hence the drag force exerted on the particles, which increases the minimum fluidization velocity. The other effect reduces the bubble size due to a decrease in viscosity and surface tension, which in turn causes decreases the minimum fluidization velocity. It is clear from Fig. 10 that the first of the above effects is the dominant one at low gas velocities; however, the relative importance of the second one seems to increase with gas velocity.

There are several correlations and models in the literature proposed to calculate the liquid minimum fluidization velocity,

Table 1
Correlations for U_{Lmf} in three-phase fluidization

References	Correlation	
[19]	$U_{Lmf} = U^{o}_{Lmf}(1 - 0.5U_G^{0.075} - \varepsilon_{mf}\beta_{Gmf})$	(16)
[20]	$U_{Lmf} = 5.359 \times 10^{-17} U_G^{-0.14} \mu_L^{-0.497} d_c^{-0.423} \rho_S^{3.75}$	(17)
[21]	$Re_{Lmf} = 0.00512 Ar_L^{0.662} Fr_G^{-0.118}$	(18a)
[21]	$U_{Lmf} = U^{o}_{Lmf}(1 - 1.62 \times 10^{3} U_G^{0.436} \mu_L^{0.227} d_v^{0.598} (\rho_S - \rho_L)^{-0.305})$	(18b)
[22]	$U_{Lmf} = 0.427 U_G^{-0.198} d_v^{1.539} (\rho_S - \rho_L)^{0.775}$	(19)
[23]	$U_{Lmf} = 6.969 \times 10^{-4} U_G^{-0.328} \mu_L^{-0.355} (\phi d_v)^{1.086} d_c^{0.042} (\rho_S - \rho_L)^{0.865}$	(20)
[24]	$U_{Lmf} = U^{o}_{Lmf}(1 - 376 U_G^{0.327} \mu_L^{0.227} d_v^{0.213} (\rho_S - \rho_L)^{-0.423})$	(21)
[25]	$\ln(U_{Lmf}) = \ln(U^{o}_{Lmf}) - 13.8 Fr_G^{0.35} (\rho_S - \rho_L)^{-0.38}$	(22)
[7]	Neural network $U_{Lmf} = f(U_G; \mu_L; \phi; d_v; \rho_S - \rho_L; \sigma_L; d_v/d_c)$	(23a)
[7]	Neural network $Re_{Lmf} = f(Re_G; Ar_L; \phi d_v/d_c; Mo_L)$	(23b)

Table 2
Average absolute relative error for empirical correlations to predict U_{Lmf}

Equation	AARE	Standard deviation
(16)	0.20	0.13
(18b)	0.70	0.49
(21)	0.53	0.43
(22)	0.70	0.46

among which those presented in Table 1 are among the ones most referred to in the literature [7]. These expressions have been obtained mainly for systems operated at atmospheric pressure and room temperature, and therefore their applicability to high pressure and high temperature conditions is uncertain. In order to evaluate the prediction capacity of these equations at extreme conditions, the predictions have been contrasted with the experimental data of this work and the results presented in Table 2. This table shows the average absolute relative error (AARE) of the predictions, as well as the respective standard deviation, for the expressions that showed the smallest error. It should be pointed out that several of the correlations in Table 1 utilize the value of the minimum fluidization velocity of the corresponding liquid–solid system, U^o_{Lmf}, and so for this purpose the experimental value was used.

In general terms a relatively wide distribution of errors was obtained with the correlations in Table 1. Additionally, it was found that the higher prediction errors corresponded to those equations that are not expressed in terms of U^o_{Lmf}. Such correlations tend to predict incipient velocities higher than the experimental values, which suggest that they do not adequately take into consideration the effect of pressure and temperature on the bed hydrodynamics, something that is not surprising considering their empirical nature. On the other hand, the correlations that showed the smaller errors all refer to the incipient velocity of the liquid–solid system. Furthermore, the magnitude of the errors for these correlations has been found to be of the same order of those reported for correlations at atmospheric pressure and room temperature. As it is shown in Table 2, the correlation by Ermakova et al. [19] was found to produce the smallest errors, 20% in average which is of similar magnitude to those reported by Larachi et al. [7], of 16 and 30% average errors, respectively, for their dimensional and dimensionless correlations.

4. Conclusions

The effects of high pressure and temperature on the hydrodynamic characteristics of ebullated-bed systems have been studied. For the experimental conditions of temperature and pressure considered in the present work it has been observed that the bed expanded without contraction with gas and liquid flow rates, similarly as it occurs in systems in the dispersed bubble flow regime. In fact, the prevalence of this regime has been corroborated by an empirical correlation proposed in the present work, which shows that most of the experimental systems considered operated under such regime. This also seems to explain the reasonable bed porosity predictions obtained with the pseudo-fluid model. It appears that the effect on bubble behavior of increases in temperature and pressure both tend to extend the gas and liquid velocity ranges for the dispersed bubble flow regime. An increase in pressure tends to reduce the minimum liquid velocity as a result of its effect on bubble behavior. On the other hand, it seems that an increase in temperature has a mixed effect on such velocity due to the opposing effects that result from a reduction in the drag force on the particles and from an increase in the interstitial liquid velocity produced by higher gas holdups. Finally, a comparison between the experimental minimum fluidization velocity data and the predictions from several empirical correlations have shown that the smallest prediction errors corresponded to those expressions which are an explicit function of the minimum fluidization velocity for the liquid–solid system, as long as a reliable value for such velocity is available.

References

[1] L.-S. Fan, Gas–Liquid–Solid Fluidization Engineering, Butterworths, Boston, 1989.
[2] V.K. Bhatia, N. Epstein, in: Proceedings of International Symposium on Fluidization and its Applications Cepadues-Editions, Toulouse, 1974, p. 380.
[3] D. Blum, J.J. Toman, AIChE Symp. Ser. No. 161, 73 (1977) 115.
[4] P. Jiang, X. Luo, T.-J. Lin, L.-S. Fan, Powder Technol. 90 (1997) 103.
[5] P. Jiang, D. Arters, L.-S. Fan, Ind. Eng. Chem. Res. 31 (1992) 2322.
[6] X. Luo, P. Jiang, L.-S. Fan, AIChE J. 43 (1997) 2432.
[7] F. Larachi, I. Illiuta, O. Rival, B.P.A. Grandjean, Ind. Eng. Chem. Res. 39 (2000) 563.
[8] P. Jiang, X. Luo, T.-J. Lin, L.-S. Fan, Fluidization VIII, in: Proceedings of the 8th Eng. Foundation Conference on Fluidization, 1995, p. 433.
[9] R.S. Ruiz, F. Alonso, J. Ancheyta, Catal. Today 98 (2004) 265.
[10] R. Di Felice, Chem. Eng. Sci. 55 (2000) 3899.
[11] G.B. Wallis, One-Dimensional Two-Phase Flow, McGraw-Hill, New York, 1969.
[12] J.F. Richardson, W.N. Zaki, Trans. Inst. Chem. Eng. 32 (1954) 35.
[13] H. Schlichting, Boundary-Layer Theory, McGraw-Hill, New York, 1979.
[14] L.-S. Fan, K. Tsuchiya, Bubble Wake Dynamics in Liquids and Liquid–Solid Suspensions, Butterworths, Stoneham, MA, 1990.
[15] X. Luo, J. Zhang, K. Tsuchiya, L.-S. Fan, Chem. Eng. Sci. 52 (1997) 3693.
[16] J.-P. Zhang, J.R. Grace, N. Epstein, K.S. Lim, Chem. Eng. Sci. 52 (1997) 3979.
[17] R.C. Darton, D. Harrison, Chem. Eng. Sci. 30 (1975) 581.
[18] D.N. Rundell, R.J. Schaefer, J.K. Shou, Ind. Eng. Chem. Res. 26 (1987) 613.
[19] A. Ermakova, G.K. Ziganshin, M.G. Slin'ko, Theor. Found. Chem. Eng. 4 (1970) 84.
[20] V.R. Bloxom, J.M. Costa, J. Herranz, G.L. MacWilliam, S.R. Roth, Determination and Correlation of Hydrodynamic Variables in a Three-Phase Fluidized Bed, MIT Report N219, Oak Ridge National Laboratory, Oak Ridge, TN, 1975.
[21] J.M. Begovich, J.S. Watson, in: J.F. Davidson, D.L. Kearins (Eds.), Fluidization, Cambridge University Press, Cambridge, 1978, p. 190.
[22] Y. Fortin, Ph.D. Thesis, Institut National Polytechnique de Lorraine, Lorraine, France, 1984.
[23] N. Costa, A. De Lucas, P. Garcia, Ind. Eng. Chem. Process Des. Dev. 25 (1986) 849.
[24] G.H. Song, F. Bavarian, L.-S. Fan, R.D. Buttke, L.B. Peck, Can. J. Chem. Eng. 67 (1989) 265.
[25] S. Nacef, Ph.D. Thesis, Institut National Polytechnique de Lorraine, Lorraine, France, 1991.